DESIGN OF HIGH ROTATION FREQUENCY COMPOSITE TUBES.

O. Montagnier and Ch. Hochard

Laboratoire de Mécanique et d'Acoustique
31 chemin Joseph Aiguier, 13402 Marseille Cedex 20
e-mail : oliviermontagnier@yahoo.fr

ABSTRACT

This work relates to the sizing of subcritical and supercritical laminated composite drive shafts. The hollows drive shafts are designed to transmit the torsional load and to minimize the dynamic effects due to rotation. To meet this need, these structures must combined strength, rigidity and lightness. New high modulus carbon fibres can be adapted to a progress in this field. This work presents sizing tools for optimisation of supercritical drive shafts mounted on viscoelastic suspensions. Two items are discussed: dynamic analysis (response to forces excitation; free motion; instability), strength (buckling of thin tubes; torsional strength). Supercritical drive shafts examples made of high modulus fibres or high-strength fibres are presented.

Key Words : Composite drive shaft ; High modulus fibres ; supercritical speed

1. INTRODUCTION

This work relates to the sizing of subcritical and supercritical laminated composite drive shafts.

Composite materials drive shafts are new potential candidates in many applications [1]. Drive shafts are designed to minimize the dynamic effects due to the rotation. In the case of a subcritical drive shaft, the first critical speed (which is given in a first approximation by Eq. 1) must not be reached, and this structure must therefore be both stiff along the rotational axis and lightweight.

$$f = \frac{\pi^2}{L^2}\sqrt{\frac{EI}{\rho S}} \tag{1}$$

where: I is the bending moment of inertia, S the tube section surface, E the modulus along tube axis, L the tube length and ρ the material density.

A high specific rigidity (modulus/density), typical of carbon/epoxy materials, makes it possible to increase the first critical speed or to produce longer subcritical drive shaft. When there is no satisfactory subcritical solution, which can be the case of helicopter rear drive shaft, the solution can be supercritical. In this case, the angular frequency is higher than the first critical speed (Eq.1). The design is more complex; it is necessary to know what happens when the shaft goes through a critical speed (transient motion) and to know the stability. It is also necessary to optimise the position of the eigen frequencies. It can be noted that lightness minimizes also rotational inertia.

Of course, drive shafts are also sizing to transmit the torsional load. In the case of hollow laminated composite tubes (thin-walled tubes), the drive shaft must be both resistant and stiff in torsion due to the risk of torsional buckling.

The emergence of high modulus carbon fibres for a reduced cost can be adapted to this application. Indeed, a quasi-isotropic ($[0°,90°,45°,-45°]_S$) material reinforced with Dialead K63712 fibres is twice as stiff as aluminium although its density is 1.6 times lower.
This work presents tools for drive shaft design. The objective is optimisation of drive shafts and comparison of high modulus carbon/epoxy and high resistance carbon /epoxy in this area. Two items are discussed: the dynamic performances and the strength.

2. DYNAMIC ANALYSIS

Many works relates to the analysis of the critical speeds of thin-walled composite shafts with or not supported bearings: equivalent modulus beam theory [2] ; Timoshenko beam theory with the Donnel thin shell theory [3]; finite element approach [4-5] ; shell theory of first order [6-7] ; first order shear deformable beam theory [8]. Few works investigate the transient motion and the stability of the system [9]. A study of an isotropic drive shaft on rigid supports, with a simple model of internal and external damping, shows the instability of the system for very high speeds compare to the first critical speed [10].
In this work, we investigate the problem of thin-walled composite shafts with viscoelastic supports at the ends of the tube. Our objective being optimisation of a high-speed drive shaft, we solve an analytical problem. We relate the response to force excitation, the free motion and the stability.

2.1 Modeling

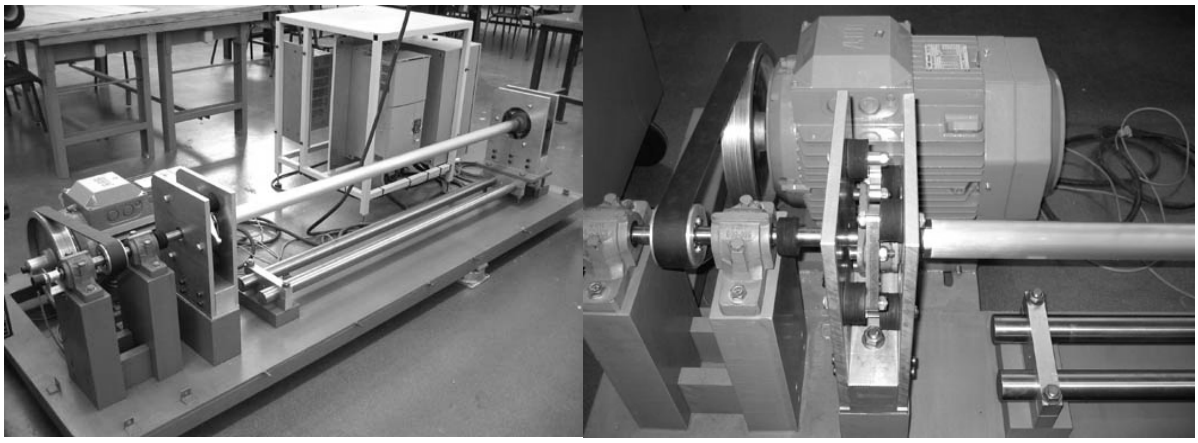

"**Fig. 1.** (a) Testing machine for high-speed tubes; (b) viscoelastic supports (natural rubber) in shear."

The modelling is issued from the original testing machine for high-speed tubes (Fig. 1. - a). The shaft is represented as a beam with a circular cross-section with simply supported ends (Fig. 2). *Oxyz* is the inertial frame. The beam theory used is the Bernoulli beam theory with an equivalent modulus. The shaft length is supposed to be great in front of the diameter. The viscoelastic support is defined by a stiffness k and a viscous damping c_e ; there are supposed to be the same in all the directions in the plane *Oxy* (Fig. 1. - b). The self-aligning ball

bearings at the ends of the tube allow us neglecting the bending of the supports. The connection between the shaft and the viscoelastic support is defined by a mass m_p.

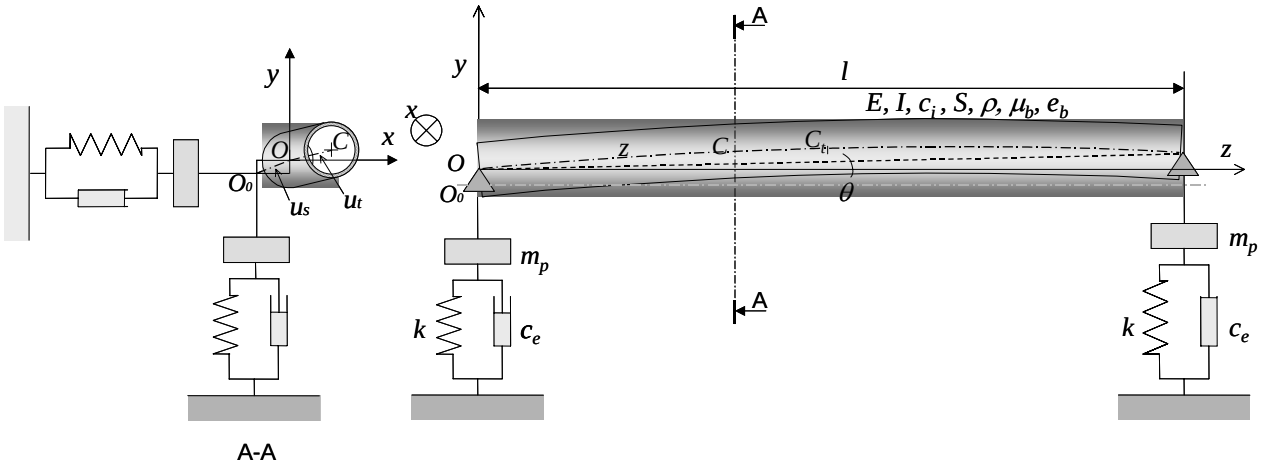

"**Fig. 2.** Shaft in rotation with viscoelastic supports."

The displacement of the tube axis is composed of a displacement u_s and a rotation θ_s (s for support). The displacement of the centre of the beam cross-section with respect to the tube axis is noted u_t. The total displacement results in:

$$u(z,t)=u_s(t)+\frac{l-2z}{2}\theta_s(t)+u_t(z,t) \qquad \forall z\in[0,l] \tag{2}$$

The local dynamic equation for the shaft in respect with the Timoshenko assumptions, including the internal viscous damping (viscous damping of the material) and neglecting the gyroscopic effect, can be written as

$$\ddot{u}+\frac{EI}{\rho S}u_t''''+\frac{c_i}{\rho S}(\dot{u}_t-i\Omega u_t)=\varepsilon\Omega^2 e^{i\Omega t} \qquad \forall z\in[0,l] \tag{3}$$

where: Ω is the angular speed, c_i the internal viscous damping and ε the distance between the inertial centre of the cross section and the tube axis (function of z) ; $f'=\partial f/\partial z$, $\dot{f}=\partial f/\partial t$.

The displacement boundary conditions are:

$$u_t''(0,t)=0\,,u_t''(l,t)=0 \tag{4}$$

$$u_t(0,t)=0\,,u_t(l,t)=0 \tag{5}$$

The dynamics equations for the viscoelastic supports are:

$$\ddot{u}_s + \frac{c_e}{m_p}\dot{u}_s + \frac{k}{m_p}u_s = -\frac{1}{2m_p}\int_0^l \rho S\left[\ddot{u} - \varepsilon\Omega^2 e^{i\Omega t}\right]dz \qquad (6)$$

$$\ddot{\theta}_s + \frac{c_e}{m_p}\dot{\theta}_s + \frac{k}{m_p}\theta_s = -\frac{1}{m_p}\int_0^l \rho S\frac{l-2z}{l^2}\left[\ddot{u} - \varepsilon\Omega^2 e^{i\Omega t}\right]dz \qquad (7)$$

2.2 Response to unbalance tube

Here only the steady-state response is calculated. The general solution is not considered. The steady-state solutions assume the displacements are in phase with the rotation ($\dot{u}_t = i\Omega u_t$) that implies the response is independent of the internal viscous damping. The local dynamic equation can be rewritten as:

$$\ddot{u} + \frac{EI}{\rho S}u_t'''' = \varepsilon\Omega^2 e^{i\Omega t} \qquad \forall z \in [0,l] \qquad (8)$$

To solve the equation system, the displacement base chosen for u_t is the exact modes shape of a beam with constant cross-section in bending, simply supported at both ends. The axis displacement is represented for the first and second modes (Fig. 3). The centre of the cross-section displacement expression is:

$$u(z,t) = \left[U_s + \frac{l-2z}{2}\Theta_s + \sum_{n=1}^{\infty} U_{tn}\sin\left(\frac{\pi n}{l}z\right)\right]e^{i\Omega t} \qquad (9)$$

where: U_s, Θ_s and U_{tn} are displacement functions of the plane Oxy (complex number), and n number of the mode.

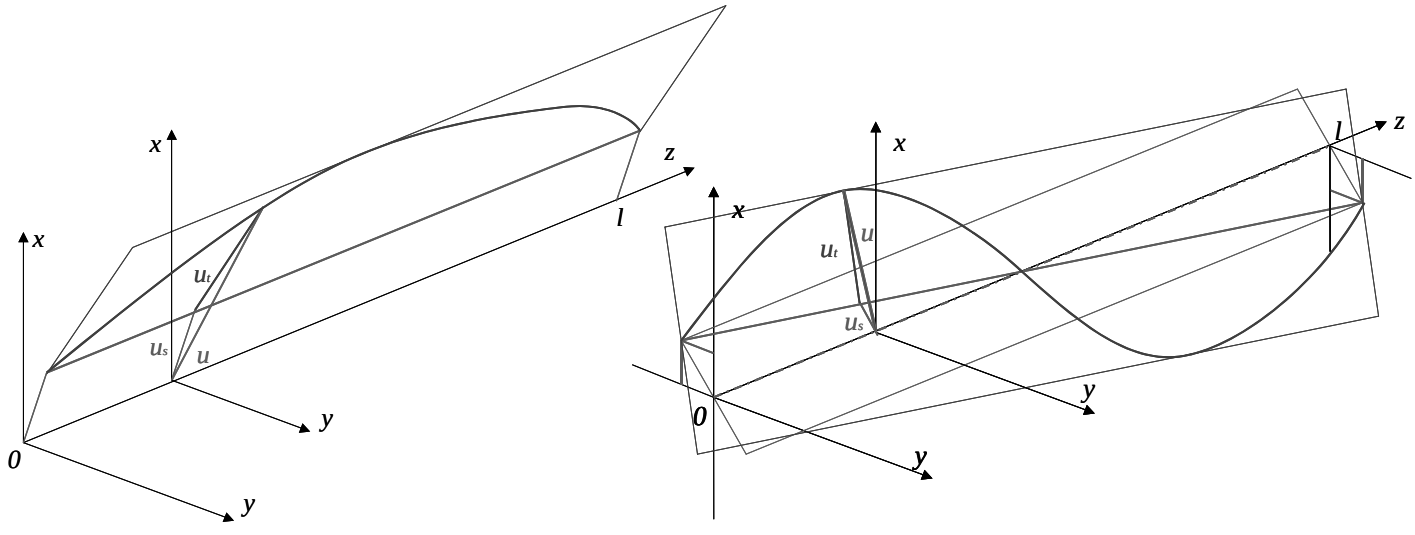

(a) (b)

"**Fig. 3.** Response to unbalance tube: near the first mode (a) and near the second mode (b)."

The equation system has been solved with the virtual work principle. We supposed that the eigen frequencies are enough separate to assume mode independency. Thus, the unbalance response can be written as:

$$\begin{cases} U_{tn}=\dfrac{2}{l}\dfrac{\Omega^2\left[\ \left[-\Omega^2+A_{eu}i\Omega+\omega_{0u}^2\right]\int_0^l \varepsilon\sin(\frac{\pi n}{l}z)dz+\Omega^2\frac{r_{mu}}{n\pi}\int_0^l\varepsilon dz\ \right]}{(\Omega_n^2-\Omega^2)\left[-\Omega^2+A_{eu}i\Omega+\omega_{0u}^2\right]-\Omega^4\dfrac{4r_{mu}}{(n\pi)^2}} & \text{if } n \text{ is odd} \quad (10) \\ U_{tn}=\dfrac{2}{l}\dfrac{\Omega^2\left[\ \left[-\Omega^2+A_{e\theta}i\Omega+\omega_{0\theta}^2\right]\int_0^l \varepsilon\sin(\frac{\pi n}{l}z)dz+\Omega^2\frac{r_{m\theta}}{n\pi}\int_0^l(1-2\frac{z}{l})\varepsilon dz\ \right]}{(\Omega_n^2-\Omega^2)\left[-\Omega^2+A_{e\theta}i\Omega+\omega_{0\theta}^2\right]-\Omega^4\dfrac{4r_{m\theta}}{(n\pi)^2}} & \text{if } n \text{ is even} \quad (11) \\ U_s=\dfrac{r_{mu}\Omega^2}{-\Omega^2+A_{eu}i\Omega+\omega_{0u}^2}\left[\sum_{n\ impair}\frac{1}{n\pi}U_{tn}+\frac{1}{2l}\int_0^l\varepsilon dz\right] & (12) \\ \Theta_s=\dfrac{2}{l}\dfrac{r_{m\theta}\Omega^2}{-\Omega^2+A_{e\theta}i\Omega+\omega_{0\theta}^2}\left[\sum_{n\ pair}\frac{1}{n\pi}U_{tn}+\frac{1}{2l}\int_0^l(1-2\frac{z}{l})\varepsilon dz\right] & (13) \end{cases}$$

with

$$\Omega_n=2\pi f_n=(\frac{\pi n}{l})^2\sqrt{\frac{EI}{\rho S}} \quad (14)$$

$$\omega_{0u}=\sqrt{\frac{k}{\frac{m_a}{2}+m_p}},\ \omega_{0\theta}=\sqrt{\frac{k}{\frac{m_a}{6}+m_p}} \quad (15)$$

$$A_{eu}=\frac{c_e}{\frac{m_a}{2}+m_p}=2\xi_e\omega_{0u},\ A_{e\theta}=\frac{c_e}{\frac{m_a}{6}+m_p}=2\xi_e\omega_{0\theta} \quad (16)$$

$$r_{mu}=\frac{m_a}{\frac{m_a}{2}+m_p},\ r_{m\theta}=\frac{m_a}{\frac{m_a}{6}+m_p} \quad (17)$$

The internal viscous damping has no effect in the steady state solution. For the rotational speed Ω, the shaft turns bended. The mode amplitude is only governed by the external damping, the tube defects, and the geometrical parameters. Let us notice that the mode amplitude of a simply supported beam in bending is only governed by the internal damping, the excitation force and the geometrical parameters. We note here the difference between the two problems in respect with the damping.

From that solution, we deduce the n critical rotational speed (notation: $\chi=u$ if n is odd; $\chi=\theta$ if n is even):

$$\Omega_{an}^2 = \frac{\Omega_n^2 + \omega_{0\chi}^2}{2(1-\frac{4r_{m\chi}}{(n\pi)^2})}\left[1 \pm \sqrt{1-4(1-\frac{4r_{m\chi}}{(n\pi)^2})\left[\frac{\omega_{0\chi}\Omega_n}{\Omega_n^2+\omega_{0\chi}^2}\right]^2}\right] \quad (18)$$

2.3 Free motion and instability

Tondl performed the study of the stability for the case of a symmetric rotor with a disk and a viscoelastic shaft [10]. The shaft was modelling with a viscous damping and a stiffness, only the first mode was taken into account. Tondl showed the shaft instability appears when the rotational speed is superior to:

$$\Omega_{\lim} \approx \Omega_1(1+\frac{A_e}{A_i}) \quad (19)$$

where : A_e is the external viscous damping and A_i the internal viscous damping.

The author concluded that after the critical speed, the external damping is a stabilising parameter and on the other hand the internal damping is a destabilising parameter.
In our case, we used the same method to conclude about the effect of the damping parameters. Here, for the free motion, the dynamic system can be written as:

$$\begin{cases} \ddot{u} + \frac{EI}{\rho S}u_t'''' + \frac{c_i}{\rho S}(\dot{u}_t - i\Omega u_t) = 0 \quad \forall z \in [0,l] & (20) \\ \ddot{u}_s + \frac{c_e}{m_p}\dot{u}_s + \frac{k}{m_p}u_s = -\frac{\rho S}{2m_p}\int_0^l \ddot{u}dz & (21) \\ \ddot{\theta}_s + \frac{c_e}{m_p}\dot{\theta}_s + \frac{k}{m_p}\theta_s = -\frac{\rho S}{m_p}\int_0^l \frac{l-2z}{l^2}\ddot{u}dz & (22) \end{cases}$$

To solve the dynamic system, we used the same assumption on the displacements than the case of force excitation. In a classic manner, we introduced an eigen value λ_n unknown in the time function. For the transient mode *n*, the displacement expression is:

$$u(z,t) = \left[U_{sn} + \frac{l-2z}{2}\Theta_{sn} + U_{tn}\sin(\frac{\pi n}{l}z)\right]e^{i\lambda_n t} \quad (23)$$

where: U_{sn}, Θ_{sn} and U_{tn} are displacement functions of the plane *Oxy* (complex number), and λ_n the eigen frequencies of the transient mode *n* (complex number).

The equation system has been solved with the virtual work principle. We wrote the eigen frequencies with a real part and an imaginary part:

$$\lambda_n = g_n + ih_n \quad (24)$$

The equation system can be written as a simple complex equation of order 4 in λ_n:

$$\begin{aligned}\Psi_n\lambda_n^4 - i(A_{en}+A_{in})\lambda_n^3 - (\Omega_n^2+\omega_{0n}^2+A_{en}A_{in}-iA_{in}\Omega)\lambda_n^2 \\ +(A_{en}A_{in}\Omega + i(A_{in}\omega_{0n}^2+A_{en}\Omega_n^2))\lambda_n + \omega_{0n}^2\Omega_n^2 - iA_{in}\omega_{0n}^2\Omega = 0\end{aligned} \quad (25)$$

with

$$\Psi_n = 1 - \frac{4r_{m\chi}}{n^2\pi^2} \quad (26)$$

The real part of λ_n is an eigen value and the imaginary part represented a viscous damping, that implies that $g_n >> h_n$. This remark allows us to find analytical solutions approximate to the Eq. 25 and to conclude on the stability of these transient modes. For each *n*, we found two stable transient modes and two unstable. For the unstable transient modes, the instability appears when the rotational speed is superior to:

$$\Omega_{\lim\_n3} = \frac{g_{n3}^3}{g_{n3}^2-\omega_{0n}^2}\left(1-\frac{\omega_{0n}^2}{g_{n3}^2}+\frac{A_{en}}{A_{in}}\left(1-\frac{\Omega_n^2}{g_{n3}^2}\right)\right) \quad (27)$$

$$\Omega_{\lim\_n4} = \frac{g_{n4}^3}{g_{n4}^2-\omega_{0n}^2}\left(1-\frac{\omega_{0n}^2}{g_{n4}^2}+\frac{A_{en}}{A_{in}}\left(1-\frac{\Omega_n^2}{g_{n4}^2}\right)\right) \quad (28)$$

with

$$g_{n3} = \frac{1}{\sqrt{2\Psi_n}}\sqrt{\Omega_n^2+\omega_{0n}^2-\sqrt{\Omega_n^4+2(1-2\Psi_n)\Omega_n^2\omega_{0n}^2+\omega_{0n}^4}} \quad (29)$$

$$g_{n4} = \frac{1}{\sqrt{2\Psi_n}}\sqrt{\Omega_n^2+\omega_{0n}^2+\sqrt{\Omega_n^4+2(1-2\Psi_n)\Omega_n^2\omega_{0n}^2+\omega_{0n}^4}} \quad (30)$$

It is then enough to determine the frequency limit lowest to conclude. We find in our case of, the result obtained by Tondl on a simplified rotor (Eq. 19), which is the external damping is a stabilising parameter and the internal damping is a destabilising parameter.

2.4 Internal viscous damping

The calculation of internal viscous damping (noted ξ_i) was carried out starting from an strain energy approach carried out by Ni et al. [11] and Adams [12]. This theory was applied to the laminates theory. The strain energy is calculated by separating energy in the longitudinal direction, in the transverse direction and in shear. Dissipated energy is calculated by multiplying each of the three energies by the corresponding damping. The damping is obtained by dividing the dissipated energy by the strain energy. The damping which appears in the stability problem (2.3) is given by the traction of the laminate according to the tube axis. The frequency response of the viscoelastic properties is not taken into account.

3. TORSION BUCKLING AND STRENGTH

3.1 Torsion Buckling of hollow laminated composite shaft

For the case of isotropic materials, Flügge carried out the analytical calculation of the buckling moment in torsion (noted $C_{buckling}$) of thin-walled tubes with the assumption of tubes infinitely long [13]. This assumption supposes that the end effects are negligible. This solution correlates the experimental results of Donnel [14] with an error lower than 10% when the thin tube length is at least forty times higher than the diameter. Here, for the case of the carbon/epoxy materials, the theory of the laminates is associated to the Flügge thin shell theory. This method is presented in works of Bert et al. [15]. On the other hand, we used the assumption of tubes infinitely long to calculate a quasi-analytical solution (minimisation of a determinant), which does not require iterative calculations expensive in time.

3.2 Strength

We limit ourselves to an application of supercritical drive shaft where the shaft goes through a critical speed within significant torque. The problems of bending and torsion are dissociated. In practice, for the case of helicopter rear supercritical drive shafts, the rotational speed increasing until the nominal speed is carried out during the launching phase.

The rupture torque (noted $C_{Tsai\text{-}Wu}$) is calculated by the Tsai-Wu criterion. This approach is however insufficient. The behaviour of the carbon/epoxy composite being non-linear particularly in compression, works must be directed towards a more complete calculation in strength. The measurement of behaviour in compression was carried out by a new pure bending test [16].

4. EXAMPLE: COMPARISON OF HIGH MODULUS CARBON FIBRES / HIGH RESISTANCE CARBON FIBRES

The study is carried out with a shaft length, a thickness and a diameter known (L=2m, e=1.5mm,D=80mm). For the computation, the connection mass m_p is 3kg, the shaft defect ε is 0.1mm, the support stiffness k is $4{,}8.10^5$N/m and the external viscous damping ξ_e is 5%.

The carbon/epoxy unidirectional materials compared are the T300/G947 (high resistance fibres) and the Dialead® K63712/R367-2 (high modulus fibres) (Table 1). Traditional measures of viscous damping are carried out on T300 material; these values are also used for the K63712. The studied laminates are representative of a population of tubes in carbon/epoxy, of the same thickness, adapted to the case of a transmission power (Table 2).

"Table 1. Material characteristics (V_f=0.6)."

Material	d	E_t	E_l	G_{lt}	ν_{lt}	X	X'	Y	Y'	S	h	ξ_L	ξ_T	ξ_{LT}
		GPa	GPa	GPa		Mpa	MPa	MPa	MPa	MPa	mm	%	%	%
K63712	1.70	370	5.4	4.0	0.3	1500	470	35	200	75	0.25	0.11	0.58	0.80
T300	1.53	130	9.3	4.6	0.3	1650	1650	70	215	100	0.25	0.11	0.58	0.80

The steady-state solution (Eq.10-13) revealed two peaks corresponding to the rigid mode (f_0 ≈63Hz; Eq. 12) and to the first shaft bending mode. When these two frequencies are distinct, the bending mode is largely prevalent in amplitude (Fig. 4 (a)). The rigid mode is negligible. If the frequency of the rigid mode is close to the first Eigen frequency (Fig. 4 (b)), the effect of external damping is amplified what implies a disappearance of the peak. The amplitude of the two peaks is very low.

The results present the prevalent mode in amplitude (Tab. 2). The displacement of the mass and the tube centre displacement for the first mode are respectively noted U_s and U_t.

"**Table 2.** Mechanical and dynamics characteristics of laminate tubes."

Laminate (/*x*)		Material	$C_{Tsai\text{-}Wu}$	$C_{buckling}$	E	f	U_s	U_t	ξ_i
			N.m	N.m	GPa	Hz	mm	mm	%
$[45,-45]_3$	1	T300	6030	947	16.3	34.5	1.20	22.8	0.73
	2	K63712	2332	2015	15.4	31.8	1.38	29.5	0.77
$[30,-30]_3$	3	T300	4578	681	45.0	50.7	0.43	1.54	0.46
	4	K63712	2032	1066	54.9	76.6	0.35	1.32	0.62
$[15,-15]_3$	5	T300	2768	832	106	101	0.89	5.65	0.18
	6	K63712	1278	1739	248	145	1.70	12.4	0.24
[45,15,-15,-45,-15,15]	7	T300	1955	1038	76	88.2	0.62	3.27	0.21
	8	K63712	1161	2472	193	128	1.40	9.74	0.16
$[0_2,45,-45,0_2]$	9	T300	2323	821	93.1	95.9	0.78	4.65	0.15
	10	K63712	842	1866	253	146	1.72	12.6	0.13
[0,90,45,-45,90,0]	11	T300	2797	1131	57.8	79.8	0.43	1.86	0.18
	12	K63712	1094	2787	152	115	1.15	7.51	0.15
[45,-45,0,90,-45,45]	13	T300	4936	1214	41.0	49.5	0.47	2.02	0.26
	14	K63712	2129	2995	99.5	95.3	0.77	4.18	0.17

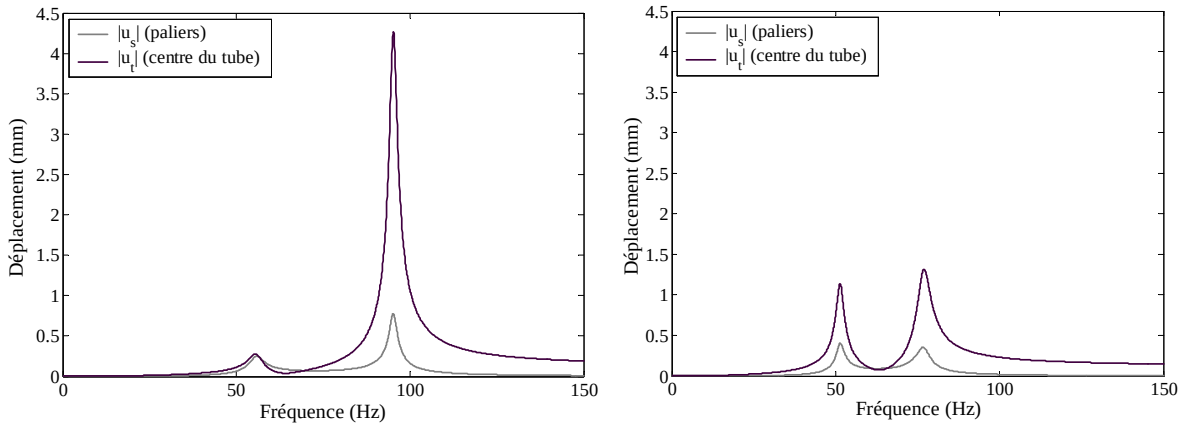

"Fig. 4. Steady-state solution for unbalance composite tubes: 14 (f_1=83Hz) (a) and 13 (b) (f_1=62Hz)."

The tubes made of high modulus fibres have a good behaviour in respect with buckling. For these tubes, the rupture is material type. The tubes made of high strength fibres break in buckling, the ratio thickness/diameter being particularly weak in this example.
For this kind of tubes (diameter and thickness imposed), the high modulus fibres offer overall better performances. This first stage being qualitative, a stage of optimisation is necessary.

5. CONCLUSIONS

This work highlights some points of the sizing of subcritical and supercritical drive shafts in carbon/epoxy composite. The high modulus fibres are particularly penalized by their low

resistance in compression. The laminates used are not optimal, the maximum couple being generally reached in only one direction. Low resistance in compression can be optimising by a greater number of folds with -45°. The load of the unbalance being proportional at its square speed, the optimisation of a supercritical problem will have to minimize the magnitude of the peaks by carrying out a good distribution of the eigen frequencies. The optimal solution will have to also check the dynamic stability of the system. Let us notice that the increase in rigidity is associated to a reduction of the internal damping.

Références

1. **Faust, H., Mack, J.** and **Spencer, B.**, "A composite rotor shaft for the Chinook", *Journal of the American Helicopter Society*, **29** (1984), 54-58.
2. **Zinberg, H.,** and **Symonds, M.F.,** "The Development of an Advanced Composite Tail Rotor Driveshaft", *Presented at the 26th Annual Forum of the American helicopter Society*, Washington, DC (1970).
3. **dos Reis, H.L.M., Goldman, R.B.,** and **Verstrate, P.H.,**. "Thin-walled laminated composite cylindrical tubes: Part III—Critical speed analysis", *Journal of Composites Technology and Research*, **9** (1987), 58–62.
4. **Ruhl, R.L.,** and **Booker, J.F.,**. "A finite element model for distributed parameter turborotor systems", *Journal of Engineering for Industry* (1972), 126–132.
5. **Lalanne, M.,** and **Ferraris,G.,** « Rotordynamics prediction in engineering », *Wiley*, 2nd edition (1998).
6. **Kim, C.D.,** and **Bert, C.W.,** "Critical speed analysis of laminated composite, hollow drive shafts", *Composites Engineering*, **3** (1993), 633–643.
7. **Shabaneh, N.H.,** and **Zu, J.W.,** "Dynamic analysis of rotor-shaft systems with viscoelastically supported bearings", *Mechanism and machine theory*, University of Toronto, **35** (2000), 1313-1330.
8. **Chang, M. Y., Chen, J.K.** and **Chang, C.Y.**, ″A simple spinning laminated composite shaft model″, *International Journal of Solids and Structures*, **41** (2004), 637-662.
9. **Song, O., Jeong, N.-H.,** and **Librescu, L.,** "Implication of conservative and gyroscopic forces on vibration and stability of an elastically tailored rotating shaft modeled as a composite thin-walled beam", *Journal of Acoustical Society of America* **109** (3) (2001), 972–981.
10. **Tondl, A.**, ″Some problems of rotor dynamics", *Czechoslovak academy of sciences*, Prague, (1965).
11. **Ni, R. G.** and **Adams, R. D.**, ″A rational method for obtaining the dynamic mechanical properties of laminae for prediction of the damping of laminated plates and beams″, *Composites*, **15** (1984), 193-199.
12. **Adams, R. D.**, ″Damping properties analysis of composites.″, *Engineering Material Handbook*, ASM, **1** (1987), 206-217.
13. **Flügge, W.**, "Stresses in shells", 2nd edn, Springer-Verlag, New-York (1973).
14. **Donnell, L. H.**, "Stability of thin-walled tubes under torsion", *NACA report 479* (1934), 95-115.
15. **Bert, C. W.** and **Kim, C.D.**, ″Analysis of buckling of hollow laminated composite drive shafts″, *Composites Science and Technology*, **53** (1995), 343-351.
16. **Montagnier, O., Hochard, C.** and **Charles, J.-P.**, ″Comportement en compression de fibres carbone à haut module″, *In Proceedings of the 13ème Journées Nationales sur les Composites*, Strasbourg, France, (2003), 891-900.